Indole-based Cyanine as a Nuclear RNA-Selective Two-Photon Fluorescent Probe for Live Cell Imaging

Guo, Lei; Chan, Miu Shan; Xu, Di; Tam, Dick Yan; Bolze, Frédéric; Lo, Pik Kwan; Wong, Man Shing

Published in:
ACS Chemical Biology

DOI:
10.1021/cb500927r

Published: 15/05/2015

Document Version:
Peer reviewed version

Indole-based Cyanine as a Nuclear RNA-Selective Two-Photon Fluorescent Probe for Live Cell Imaging

Lei Guo,[†,‡] Miu Shan Chan,[§,‡] Di Xu,[†] Dick Yan Tam,[§] Frédéric Bolze,*[,⊥] Pik Kwan Lo,*[,§] and Man Shing Wong*[,‡]

[†] Department of Chemistry and Institute of Molecular Functional Materials, Hong Kong Baptist University, 224 Waterloo Road, Hong Kong SAR., China.

[§] Department of Biology and Chemistry, City University of Hong Kong, Tat Chee Avenue, Kowloon Tong, Hong Kong SAR, China.

[⊥] Laboratoire de Conception et Application des Molécules Bioactives, UMR University of Strasbourg-CNRS 7199, Faculté de Pharmacie, Université de Strasbourg, France.

Supporting Information

ABSTRACT: We have demonstrated that the sub-cellular targeting properties of the indole-based cyanines can be tuned by the functional substituent attached onto the indole moiety in which the first example of a highly RNA-selective and two-photon active fluorescent light-up probe for high contrast and brightness TPEF images of rRNA in nucleolus of live cells has been developed. It is important to find that this cyanine binds much stronger toward RNA than DNA in buffer solution as well as selectively stains and targets to rRNA in nucleolus. Remarkably, the TPEF brightness ($\Phi\sigma_{max}$) is dramatically increased with 11-fold enhancement in the presence of rRNA leading to the record high $\Phi\sigma_{max}$ of 228 GM for RNA. This probe not only shows good biocompatibility and superior photostability but also offers general applicability to various live cell lines including HeLa, HepG2, MCF-7 and KB cells, and excellent counterstaining compatibility with commercially available DNA or protein trackers.

An insight of selective staining/imaging of specific cellular organelles is of paramount importance for a deeper understanding of the character of each component in a cellular system and their complex biological functions and processes.[1,2] Recently, there has been significant progress in developing subcellular organelle-specific probes based on small molecules and nanoparticles as invaluable tools in cell biology and medical imaging.[3-7] Among them, organelle-targeting two-photon excited fluorescence (TPEF) probes have increasingly drawn attention because of the lower-energy excitation of these probes, which offers numerous advantages including deep tissue imaging, minimal photodamage to biological samples and bleaching to the probes, and low interference from the auto-fluorescence of a cell. [8-10]

Various TPEF probes have been successfully designed and synthesized for mitochondria, lysosomes, and cell membrane targeting in the past few years.[11-14] Recently, Teulade-Fichou *et al.* reported a nuclear membrane permeable DNA-selective TPEF probe which bound to duplex DNA in nucleus due to its relatively strong interaction with DNA at the AT-rich region. [15] This probe allowed the investigation of the transcriptional dynamics of the cell nucleus. However, a nuclear RNA-selective TPEF probe for live cell imaging is rarely available. The vast majority of investigations of sophisticated dynamics of RNA distribution in relation to the higher-order structural organization of DNA, as well as the spatial and temporal transportation and processing of RNA molecules in the cell nucleus are not currently feasible without using genetically modified protocols.[16-19] It is known that cell growth and proliferation are greatly related to the functions of ribosomal RNA (rRNA) in nucleus.[20] Therefore, it is highly desirable to develop a RNA-selective TPEF probe to stain RNA and image nucleolus in live cells, in particular for a better understanding of nucleolar dynamic mechanisms of a change in RNA content and distribution, trafficking, and localization throughout a complete cell cycle.

We report herein a series of highly two-photon absorption (TPA) active indole-based cyanine fluorophores, namely HPI, MPI and EPI, respectively (Figure 1A) for high contrast and brightness imaging in live cells and also the first successful example of effective RNA-selective TPEF light-up probe for distinct nucleolus imaging in live cells. Cyanine lead structure has been found useful as a fluorescence sensing or imaging probe because of its strong fluorescence enhancement property upon binding or enclosing in a hydrophobic environment or a viscous medium, which is due to a reduction in non-radiative decay caused by restricted torsional rotation in the excited state.[21-23] These indole-based TPEF probes were also found to be highly cell permeable and exhibit a low cytotoxicity. Interestingly, the binding and targeting property of these indole-based cyanine molecules can be easily modified/tuned by a substituent attached onto the indole moiety. It is important to

find that one of these cyanines, namely MPI exhibits much stronger binding affinity toward RNA than DNA in buffer solution and ~~also~~ selectively stains and targets to rRNA in nucleolus.[10] Remarkably, the TPEF brightness (= two photon absorption cross-section (σ_{max}) × fluorescence quantum yield *(Φ)*) of MPI was dramatically enhanced in the presence of RNA and found to be 228 GM at 900 nm, which is the highest TPEF brightness ever reported for RNA and thus affording excellent contrast and brightness of images of rRNA in nucleolus. The MPI probe also exhibits a higher photostability under one- and two-photon excitation as well as provides less background in the cytoplasm in comparison with the commercially available one-photon SYTO RNASelect probe. Furthermore, it shows a good counterstaining compatibility with other commercially available DNA staining dyes.

Table 1. Photophysical properties of indole-based cationic molecules

Cmpd	Solvent[a]	$\lambda_{abs}(\varepsilon)$[b]	λ_{em}[c]	Φ/(%)[d]	σ_{max}(GM) (λ_{TP}/nm)[g]	$\Phi\times\sigma_2$(GM) (λ_{TP}/nm)[h]
EPI	DMSO	439 (2.43)	546	4.5	225 (830) 760 (930)	
	T.E.	420 (2.48)	540	0.67		19 (900)
HPI	DMSO	431 (2.71)	544	4.0	344 (820) 779 (930)	
	T.E.	437 (2.72)	544	0.39		21 (900)
MPI	DMSO	442 (2.63)	536	3.5	359 (820) 980 (930)	
	T.E.	429 (2.47)	547	0.55		20.4 (900)
	DNA	445	544	8.7[e]		76 (900)[i]
	RNA	458	540	17.6[f]		228 (900)[i]
Syto[j]	RNA	490	530	16.9[k]		

[a] DMSO is dimethyl sulfoxide, T.E. buffer is 10 mM Tris–HCl, 1 mM EDTA, pH = 7.5. [b] Linear absorption maximum peak in nm unit, ε is the molar absorptivity (10^4 M^{-1} cm^{-1}). [c] Fluorescence maximum peak excited at the absorption maxima in nm unit. [d] Fluorescence quantum yield using Coumarin 6 (Φ_{420} = 0.78) as the standard, ±10%. [e] Excitation at 430 nm in the presence of DNA with the ratio of phosphate of DNA:dye = 60:1. [f] Excitation at 430 nm in the presence of rRNA with the ratio (phosphate of RNA/dye) of 60:1. [g] The maximum ~~of~~ TPA cross-section using Rhodamine 6G as the standard excited at the optimized wavelength (λ_{TP}) where 1 GM = 10^{-50} $cm^4 \cdot s \cdot photon^{-1}$. The experimental error of the TPA cross-sections was determined to be ±15%. [h] Two-photon action absorption cross-section in GM unit. [i] The DNA or r-RNA to dye ratio (phosphate of NA/dye) is at 30:1 for TPA measurements. [j] Syto refers to SYTO RNASelect. [k] Excitation at 480 nm in the presence of rRNA with the ratio of phosphate of RNA:dye = 60:1 using Rhodamine 6G (Φ_{480} = 0.95) as the standard, ±10%.

The syntheses of HPI, MPI, and EPI are outlined in Supplementary Scheme S1, in which the Knoevenagel condensation was used as the key step for the synthesis of the cyanine skeleton. They were fully characterized by ^{1}H NMR, ^{13}C NMR, HRMS and elemental analysis. The data obtained are in good agreement with the proposed structures. The photophysical properties of the three cyanines are summarized in Table 1. All of the indole-based cyanines were very soluble in common polar organic solvents and aqueous buffer. They showed very similar absorption and fluorescence characteristics in, DMSO or T.E. buffer (10 mM Tis-HCl, 1 mM EDTA, pH = 7.5) (Supplementary Figure S2). Upon excitation at their absorption maxima, these cyanines exhibit relatively strong fluorescence in the range of 536–546 nm in DMSO but very weak emission and low fluorescence quantum yield in aqueous medium which is attributed to the very rapid non-radiative decay caused by the strong and dynamic adhesive interactions with water molecules.[24] Nevertheless, upon binding to nucleic acid such as calf thymus DNA (ct-DNA) or 16S and 23S ribosomal RNA (rRNA), these cyanines would exhibit a significant spectral shift and strong fluorescence enhancement, particularly for the binding of MPI with rRNA showing more than 26-fold fluorescence enhancement (Supplementary Figure S3a) and 32-fold increase in fluorescence quantum yield (Table 1). This property is especially beneficial to the application of imaging of RNA distribution in a cellular environment.

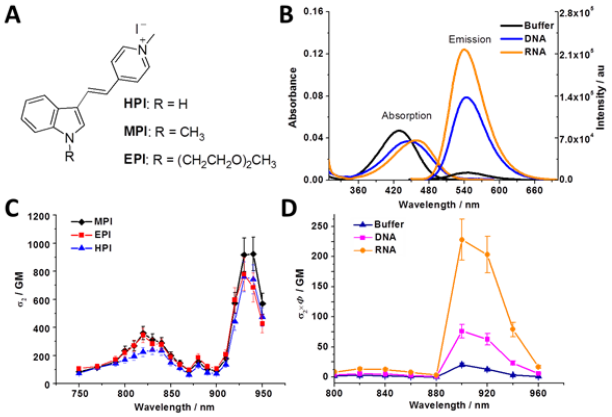

Figure 1. A) Molecular structures of HPI, MPI, and EPI. B) Linear absorption and emission spectra of MPI without or with calf thymus DNA (ct-DNA) or 16S and 32S rRNA in T.E. buffer at pH 7.5 with the ratio of phosphate of NA:dye = 60:1 and [MPI] = 1.9 μM. C) Two-photon excitation spectra of MPI, HPI and EPI measured in DMSO. D) Two-photon excitation spectra of TPEF brightness of MPI in the presence of DNA and RNA measured in T.E. buffer solution with the ratio of phosphate of NA:dye = 30:1.

To determine the binding characteristics of these cyanines with nucleic acids in T.E. buffer at pH 7.5, the fluorescence titration was carried out.[25,26] A plot of fluorescence intensity of MPI as a function of concentration of DNA and RNA was shown in Supplementary Figure S4. The dissociation constant (K_d) of MPI to DNA as estimated by the nonlinear curve fitting analysis of the fluorescence titration data was found to be 79 μM indicating relatively strong binding interaction between them; however, HPI and EPI could only exhibit an extremely weak binding affinity toward DNA with K_d = 14.9 mM and 22.8 mM, respectively (Supplementary Figure S4). These findings suggest that a variation of substituent attached at the indole moiety can greatly vary the hydrophilic-lipophilic balance of these cationic molecules and thus providing a tool to fine-tune the binding interaction with DNA. Furthermore, MPI showed exceptionally strong interaction with rRNA with K_d = 22 μM, which was more than 3-time binding stronger than ct-DNA and comparable to that of commercially available RNA-staining dye, SYTO RNASelect (K_d = 17 μM for RNA and K_d = 1.2 μM for DNA). With such a strong rRNA binding affinity

and a large fluorescence intensity enhancement upon RNA binding, MPI is potentially useful as a rRNA-selective fluorescent probe for tracking an organelle where it contains RNA components.

Upon excitation at 820 or 930 nm femtosecond (fs) laser pulses in DMSO, strong fluorescence peaked at ~540 nm was observed. The conventional TPEF method using a femtosecond pulsed laser was used to determine the TPA cross-sections and two-photon excited (TPE) spectra for these indole-based cyanines in the range of 750–950 nm in DMSO (Figure 1C and Table 1). These cyanines showed very similar TPE spectra with a maximum TPA cross-section (σ_{max}) of 980, 760, and 780 GM for MPI, EPI, and HPI at 930 nm, respectively. The power-squared dependence of TPEF of these cyanines at 930 nm fs laser pulse was followed with the slope of ~1.9, confirming that this was a two-photon excitation process (Supplementary Figure S5). As shown in Figure 1D, the TPEF brightness ($\Phi\sigma_{max}$) of MPI with rRNA in T.E. buffer solution is much stronger than that of MPI with ct-DNA under the same phosphate per nuclear acid/MPI ratio, consistent to the stronger binding affinity with rRNA. The maximum TPEF brightness ($\Phi\sigma_{max}$) of MPI in the presence of ct-DNA and rRNA (1:30) are 76 GM and 228 GM at 900 nm, respectively, which is an 11-fold enhancement compared with that without rRNA. These findings strongly suggest that MPI exhibiting a dramatically enhanced TPEF brightness upon binding to RNA can be used as a RNA-selective TPEF light-up probe for nucleoli imaging.

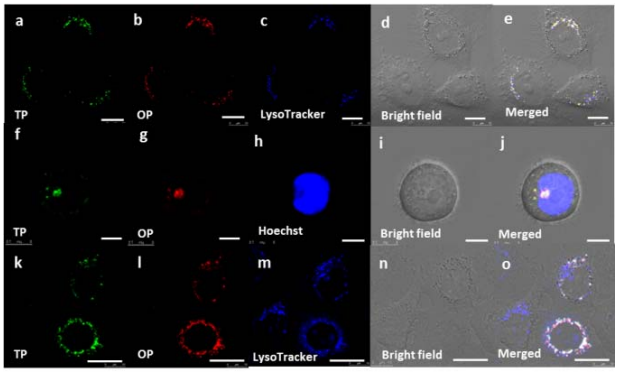

Figure 2. Colocalized fluorescence images of HeLa cells after incubation with 23 μM of (a-e) HPI, (f-j) MPI and (k-o) EPI in the presence of different organelle trackers. TP images were obtained by excitation at 880 nm. Scale bar is 10 μm.

To determine the sub-cellular targeting property of these indole-based cyanines, the colocalization of these molecules with various organelle trackers including Mito Tracker Green, Lyso Tracker Green, Endo Tracker Green, and nuclei Tracker Hoechst in HeLa cells was carried out. The one-photon (OP) and two-photon (TP) excited fluorescence images showed that all three probes were efficiently taken up by HeLa cells at a concentration of 23 μM in PBS buffer at pH 7.4 affording high contrast and bright images (Figure 2 and Supplementary Figure S6). Interestingly, the fluorescence images of HPI greatly overlapped with that of the Lyso Tracker indicating that HPI ~~is~~ localized in lysosome (Figure 2a-e); in sharp contrast, the fluorescence images of EPI did not overlap with any organelle trackers indicating that EPI distributed randomly in cytoplasm only (Figure 2k-o). Remarkably, the fluorescence images of MPI and Hoechst dye were observed in the same region suggesting that the intracellular localization of MPI was in the nucleus (Figure 2f-j). Thus, because of the ease of modifying the substituent attached onto indole moiety, the targeting and localization properties can be easily tuned and optimized for this cyanine molecule as an effective organelle specific TP fluorescent probe.

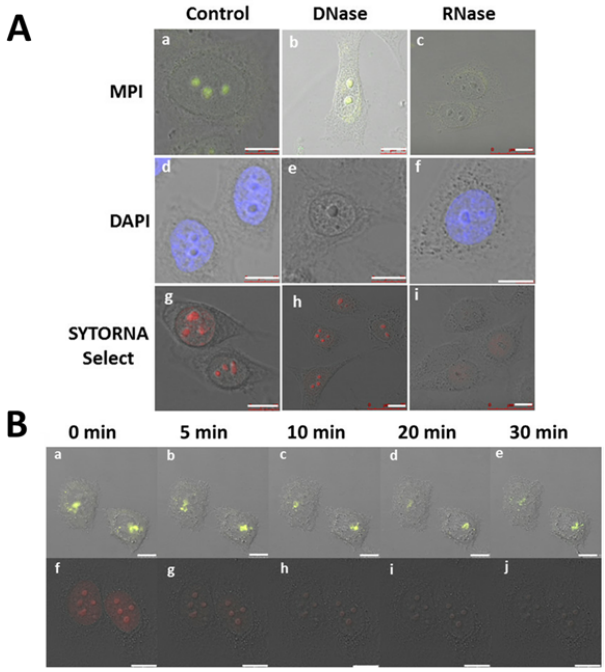

Figure 3. A) Confocal fluorescence signals of MPI, DAPI and SYTO RNASelect (a, d, g) before and after the (b, e, h) DNase or (c, f, i) RNase treatment in fixed-permeabilized HeLa cells. B) HeLa cells stained by (a-e) MPI and (f-j) SYTORNASelect in PBS buffer at pH 7.4 observed by the confocal microscopy over a time lapse of 30 min. Scale bar is 10 μm.

The three-dimensional confocal fluorescence images of MPI further ascertained that MPI clearly localized inside the nucleus rather than on its surface (Supplementary Figure S7). Nevertheless, MPI did not actually overlap with DNA-selective Hoechst dye even though they both localized in nucleus. As MPI interacts stronger to RNA than DNA, it would have had a high tendency of binding to RNA and preferentially localizing in nucleolus. To confirm the ability of MPI to selectively stain RNA in nucleolus, ribonuclease (RNase) and deoxyribonuclease (DNase) digestion experiments were carried out (Figure 3). As anticipated, the TP (or OP) excited fluorescence of MPI dramatically diminished in the RNase digestion test in fixed-permeabilized cells (Figure 3A (c)) while the fluorescence intensity remained almost the same after the DNase treatment (Figure 3A (b)) and thus univocally affirmed the selective RNA targeting property of MPI in nucleus. In a control experiment, DAPI and SYTO RNASelect were tested in fixed-permeabilized HeLa cells. The DNA selective DAPI dye showed obvious intensity diminishing in the DNase treatment while RNA-selective SYTO RNASelect dye exhibited a dramatic decrease in fluorescence in the RNase treatment. In sharp contrast to MPI, SYTO RNASelect dye can only stain

RNA in the cytoplasm with merely little staining in the nucleus of live cells (Supplementary Figure S8). Thus, MPI probe shows superior performance in live cell imaging experiment, which selectively binds to RNA in nucleolus of live cells. This is the first example of TP fluorescent probe for live cell RNA imaging in nucleolus.

To ascertain the potential application of indole-based cyanine probes as organelle trackers, an MTT (3-(4,5-dimethylthiazol-2-yl)-2,5-diphenyltetrazolium bromide) assay was performed to evaluate their cytotoxicity (Supplementary Figure S9). It was revealed that more than 80% of HeLa cells survived after incubation with HPI, EPI and MPI in all concentrations except with 45.8 μM of MPI. Since MPI binds strongly to rRNA, it would not be surprised to see a sign of cytotoxicity at a high concentration. Nevertheless, the low cytotoxicity at working concentration e.g. 23 μM ensures the applicability of MPI as an organelle-targetable probe/tracker for imaging RNA distribution within live cells.

To evaluate the general applicability of the RNA-selective MPI probe, we also performed the imaging study using HepG2 (liver cancer), MCF-7 and KB cells in which MPI consistently showed the ability to pass through the nuclear membrane and to localize in nucleolus (Supplementary Figure S10). Thus, this two-photon MPI probes can be widely applied in different cell lines for RNA detection and nucleolus targeting. To investigate the counterstaining compatibility of MPI with DNA staining dye or protein, HeLa cells were treated with both MPI and DAPI or Histone 2B-RFP dye simultaneously. In these co-staining experiments, it was found that the TP or OP excited fluorescence of MPI in nucleolus and OP excited emission of DAPI (Supplementary Figure S11a-e) or Histone 2B-RFP dye (Supplementary Figure S11f-j) in nucleoplasm were clearly visualized in different excitation and emission channels. Such outstanding counterstaining compatibility of MPI probe with DAPI or Histone 2B-RFP dye would be definitely helpful in the imaging of DNA/chromatin and RNA distribution simultaneously.

Moreover, the MPI probe showed a remarkable photostability in cells under OP and TP excitation as their fluorescence signals remained stable over a period of 30 min (Figure 3B (a-e)); in sharp contrast, the fluorescence intensity of the STYO RNASelect dye (Figure 3B (f-j)) faded out in less than 10 min indicating its inappropriate use for long-time bio-imaging.

In summary, we have demonstrated that the sub-cellular targeting properties of the indole-based cyanines can be tuned by the substituent attached onto the indole moiety in which a highly nuclear rRNA selective turn-on fluorophore has been developed. Our results also reveal that the indole-based cyanine fluorophores exhibit excellent biocompatibility in terms of low cytotoxic effect, high cell permeability to live cells and superior photostability, which are essential to be used as fluorescent trackers in live cells. Importantly, one of these cyanines, namely MPI was found to bind more than 3-fold stronger to RNA than DNA in buffer solution and to selectively stain/target RNA in nuclei of live cells. In addition, MPI is highly two-photon absorption active with σ_{max} of 980 GM at 930 nm in DMSO. Remarkably, the TPEF brightness ($\Phi\sigma_{max}$) is dramatically increased in the presence of rRNA giving rise to the record high $\Phi\sigma_{max}$ of 228 GM and thus affording high contrast and brightness TPEF images of rRNA in nucleolus of live cells. Furthermore, this RNA-selective probe shows excellent counterstaining compatibility with commercially available DNA or protein trackers in nuclei. Our findings have demonstrated that MPI is a highly effective RNA-selective TPEF light-up probe for distinct nucleolus imaging in live cells.

METHODS

See Supporting Information for a detailed description of the experimental methods.

ASSOCIATED CONTENT

Supporting Information

Details of photophysical characterization, two-photon absorption measurements and results as well as cell culture and staining. This material is available free of charge via the Internet at http://pubs.acs.org.

AUTHOR INFORMATION

Corresponding Author

*E-mail: mswong@hkbu.edu.hk.
*E-mail: peggylo@cityu.edu.hk.
*E-mail: frederic.bolze@unistra.fr.

Author Contributions

‡ These authors contributed equally.

Notes

The authors declare no competing financial interest

ACKNOWLEDGMENT

This work was financially supported by GRF (HKBU 203212), Hong Kong Research Grant Council, FRG (FRG2/13-14/059), Hong Kong Baptist University, the PROCORE-France/Hong Kong Joint Research Scheme sponsored by the Research Grants Council of Hong Kong and the Consulate General of France in Hong Kong, F-HK010/127 and Institute of Molecular Functional Materials which was supported by a grant from the University Grants Committee, Areas of Excellence Scheme (AoE/P-03/08). This work was also supported by CityU Strategic Research Grant 9616302 and 7004026, and National Science Foundation of China 21324077.

REFERENCES

(1) Lodish, H., Berk, A., Zipursky, S. L., Matsudaira, P., Baltimore, D., and Darnell, J. (2000) Biomembranes and the Subcellular Organization of Eukaryotic Cells, in *Molecular Cell Biology,* (Freeman,W. H., Ed.) 4th ed., chapter 5, New York.

(2) Buchwalow, I. B., and Böcker, W. (2010) in *Immunohistochemistry: Basics and Methods*, Springer Berlin Heidelberg, pp 83–93.

(3) Kikuchi, K. (2010) Design, synthesis and biological application of chemical probes for bio-imaging. *Chem. Soc. Rev. 39*, 2048–2053.

(4) Vendrell, M., Zhai, D., Er, J. C., and Chang, Y. T. (2012) Combinatorial strategies in fluorescent probe development. *Chem. Rev. 112*, 4391–4420.

(5) Kobayashi, H., Ogawa, M., Alford, R., Choyke, P. L., and Urano,Y. (2010) New strategies for fluorescent probe design in medical diagnostic imaging. *Chem. Rev. 110*, 2620–2640.

(6) Stender, A. S., Marchuk, K., Liu, C., Sander, S., Meyer, M. W., Smith, E. A., Neupane, B., Wang, G., Li, J., Cheng, J. X., Huang, B., and Fang, N. (2013) Single cell optical imaging and spectroscopy. *Chem. Rev. 113*, 2469–2527.

(7) Yu, Z., Schmaltz, R. M., Bozeman, T. C., Paul, R., Rishel, M. J., Tsosie, K. S., and Hecht, S. M. (2013) Selective tumor cell target-

ing by the disaccharide moiety of bleomycin. *J. Am. Chem. Soc. 135*, 2883–2886.

(8) Masters, B. R. (2006) in *Confocal microscopy and multiphoton excitation microscopy: the genesis of live cell imaging*, Bellingham, Wash. SPIE.

(9) So, P. T. C., Dong, C. Y., Masters, B. R., and Berland, K. M. (2000) Two-photon excitation fluorescence microscopy. *Annu. Rev. Biomed. Eng. 2*, 399–429.

(10) Guo, L., and Wong, M. S. (2014) Multiphoton excited fluorescent materials for frequency upconversion emission and fluorescent probes. *Adv. Mater. 26*, 5400–5428.

(11) Kim, H. M., Jeong, B. H., Hyon, J. Y., An, M. J., Seo, M. S., Hong, J. H., Lee, K. J., Kim, C. H., Joo, T., Hong, S. C., and Cho, B. R. (2008) Two-photon fluorescent turn-on probe for lipid rafts in live cell and tissue. *J. Am. Chem. Soc. 130*, 4246–4247.

(12) Wang, X., Nguyen, D. M., Yanez, C. O., Rodriguez, L., Ahn, H. Y., Bonder, M. V., and Belfield, K. D. (2010) High-fidelity hydrophilic probe for two-photon fluorescence lysosomal imaging. *J. Am. Chem. Soc. 132*, 12237-12239.

(13) Han, J. H., Park, S. K., Lim, C. S., Park, M. K., Kim, H. J., Kim, H. M., and Cho, B. R. (2012) Simultaneous imaging of mitochondria and lysosomes by using two-photon fluorescent probes. *Chem. Eur. J. 18*, 15246–15249.

(14) Yang, W., Chan, P. S., Chan, M. S., Li, K. F., Lo, P. K., Mak, N. K., Cheah, K. W., and Wong, M. S. (2013) Two-photon fluorescence probes for imaging of mitochondria and lysosomes. *Chem. Commun. 49*, 3428–3430.

(15) Dumat, B., Bordeau, G., Faurel-Paul, E., Mahuteau-Betzer, F., Saettel, N., Metgé, G., Fiorini-Debuisschert, C., Charra, F., and Teulade-Fichou, M.-P. (2013) DNA switches on the two-photon efficiency of an ultrabright triphenylamine fluorescent probe specific of AT regions. *J. Am. Chem. Soc. 135*, 12697–12706.

(16) Tyagi, S. (2009) Imaging intracellular RNA distribution and dynamics in living cells. *Nat. Methods. 6*, 331–338.

(17) Monroy-Contreras, R., and Vaca, L. (2011) Molecular beacons: powerful tools for imaging RNA in living cells. *J. Nucleic Acids. 2011*, 1–15.

(18) Armitage, B. A. (2011) Imaging of RNA in live cells. *Curr. Opin. Chem. Biol. 15*, 806–812.

(19) Boutorine, A. S., Novopashina, D. S., Krasheninina, O. A., Nozeret, K., and Venyaminova, A. G. (2013) Fluorescent probes for nucleic Acid visualization in fixed and live cells. *Molecules 18*, 15357–15397.

(20) Clancy, S. (2008). RNA functions. *Nature Education*, *1*, 102. Retrieved from http://www.nature.com/scitable/topicpage/rna-functions-352.

(21) Feng, X. J., Wu, P. L., Bolze, F., Leung, H. W. C., Li, K. F., Mak, N. K., Kwong, D. W. J., Nicoud, J. F., Cheah, K. W., and Wong, M. S. (2010) Cyanines as new fluorescent probes for DNA detection and two-photon excited bioimaging. *Org. Lett. 12*, 2194–2197.

(22) Zhang, Y., Wang, J., Jia, P., Yu, X., Liu, H., Liu, X., Zhao, N., and Huang, B. (2010) Two-photon fluorescence imaging of DNA in living plant turbid tissue with carbazole dicationic salt. *Org. Biomol. Chem. 8*, 4582-4588.

(23) Dumat, B., Bordeau, G., Faurel-Paul, E., Mahuteau-Betzer, F., Saettel, N., Bombled, M., Metgé, G., Charra, F., Fiorini-Debuisschert, C., and Teulade-Fichou, M.-P. (2011) N-phenyl-carbazole-based two-photon fluorescent probes: strong sequence dependence of the duplex vs quadruplex selectivity. *Biochimie 93*, 1209–1218.

(24) Huang, C.; Peng, X.; Yi, D.; Qua, J., and Niu, H. (2013) Dicyanostilbene-based two-photon thermo-solvatochromic fluorescence probes with large two-photon absorption cross sections: Detection of solvent polarities, viscosities, and temperature. *Sensors and Actuators B: Chemical 182*, 521–529.

(25) Li, Q., Min, J., Ahn, Y.H., Namm, J., Kim, E. M., Lui, R., Kim, H. Y., Ji, Y., Wu, H., Wisniewski, T., and Chang, Y. T. (2007) Styryl-based compounds as potential in vivo imaging agents for beta-amyloid plaques. *ChemBioChem. 8*, 1679–1687.

(26) Yang, W., Wong, Y., Ng, O. T. W., Bai, L. P., Kwong, D. W. J., Ke, Y., Jiang, Z. H., Li, H. W., Yung, K. K. L., and Wong, M. S. (2012) Inhibition of beta-amyloid peptide aggregation by multifunctional carbazole-based fluorophores. *Angew. Chem. Int. Ed. 51*, 1804–1810.